PERGAMON

International Journal of Multiphase Flow 28 (2002) 1801–1821

International Journal of Multiphase Flow

www.elsevier.com/locate/ijmulflow

Lagrangian approach for simulating the gas-particle flow structure in a circulating fluidized bed riser

Haosheng Zhou [a], G. Flamant [a,*], D. Gauthier [a], Jidong Lu [b]

[a] *Institut de Science et de Génie des Matériaux et Procédés, CNRS-IMP, 66125 Odeillo-Font-Romeu Cédex, France*
[b] *National Laboratory of Coal Combustion, Huazhong University of Science and Technology, Wuhan, Hubei 430074, China*

Received 17 September 2001; received in revised form 18 June 2002

Abstract

Lagrangian approach is used to simulate the realistic process of cluster formation in circulating fluidized bed riser. The influence of particle properties, porosity function and gas velocity on the global particle flow structure, and the formation and development of local regions of higher particle concentration are investigated. The collision parameters govern the formation of non-homogeneous flow structure because of the difference of kinetic energy and velocity distribution. Moreover, the porosity function has a significant effect on the clusters. The gas flows preferentially into the region of high porosity, which leads to non-uniform drag force on the particles and affects strongly the particle flow structure. Examination of the cluster microstructure shows that the particle velocity in the cluster is smaller than around it. Segregation of particles with different diameter and density is also predicted.

Keywords: Circulating fluidized bed; Gas–solid flow; Particle cluster; Lagrangian simulation; Particle mixing

1. Introduction

Gas–solid reactions play an important role in processes dealing with chemistry, metallurgy, energy generation, petroleum refining, and waste treatment. In many cases, the particle loading is moderate to high (particle/gas mass flow ratio exceeds 0.1 kg/kg), and wide particle size distribution powders are used for practical and economical reasons. The particle–particle interactions

* Corresponding author.
E-mail address: flamant@imp.cnrs.fr (G. Flamant).

0301-9322/02/$ - see front matter
PII: S0301-9322(02)00049-6

and the particle size distribution are known to have significant influence on the hydrodynamics of gas solid reactions (Gauthier et al., 1999; Van Wachem et al., 2001a,b).

When a gas in vertical risers transports the particles, experimental studies have shown that they are distributed non-uniformly over the cross-section (Yerushalmi et al., 1978; Bader et al., 1988; Horio and Kuroki, 1994). To handle the complicated phenomena in vertical pneumatic transport of solids, two theoretical approaches are proposed, namely the Eulerian and the discrete particle approaches.

The Eulerian model considers the particulate phase as a continuous fluid interpenetrating and interacting with the fluid phase (Gidaspow et al., 1989; Kuipers et al., 1992). The kinetic theory of granular flow is used in the Eulerian model to offer a theoretical framework for simulating gas–solid flow with particles of different size and/or different density (Kumaran and Koch, 1993; Mathiesen et al., 2000; Van Wachem et al., 2001a,b). However, severe difficulties are encountered: first many closure laws related to the mutual interaction of particles belonging to different classes have to be formulated; moreover, the universality of the used constants is questionable (Bolio et al., 1995; Cao and Ahmadi, 1995).

With increasing computer power, discrete particle models have become very useful and versatile tools to study the dynamics of gas/particle flows. In this approach, each particle is treated by solving Lagrangian equations of motion for all the particles of the system, with a prescribed set of initial conditions. Once the flow properties and the particle properties are known, the interface quantities between both phases can be calculated. It offers a more natural way to overcome the aforementioned problems, since each individual particle is tracked in the simulation. Moreover, it provides a powerful tool to investigate the detailed phenomena at the individual particle scale and to examine local phenomena such as particle to bed (or bed to particle) heat and mass transfers. This approach was used to simulate gas–solid fluidization in the last decade. Phenomena such as bubbling, slugging and solid transport in circulating fluidized bed (CFB) can be simulated (Tsuji et al., 1993; Hoomans et al., 1996, 2001; Xu and Yu, 1997; Ouyang and Li, 1999; Helland et al., 2000; Van Wachem et al., 2001a,b). Some researchers simulated clusters in CFB. Tanaka and Tsuji (1991) investigated the cluster formation in a vertical riser and the particle-induced instability in gas–solid flows. They showed that particle–particle interactions play an important role in the cluster formation and they cause flow instabilities even when the mean concentration is about 0.5%. Tanaka and Tsuji (1991) and Yonemura et al. (1993) observed that gas velocity decrease and particle loading increase result in instability and inhomogeneity. Direct Monte Carlo model was used by Ito et al. (1998) to simulate the dynamics of clusters. The individual particle behaviour can only be obtained statistically because particle collision is described from statistics. Ouyang and Li (1999) developed a particle-motion-resolved discrete model to simulate heterogeneous structure in gas–solid fluidization. Helland et al. (2000) studied the cluster formation in gas-particle CFB. They studied the influence of porosity function and observed large difference of the local flow as a function of porosity.

Great achievements have been made to simulate the cluster formation in the CFB riser. However, to simulate the cluster formation, several researchers (Tanaka et al., 1995; Ito et al., 1998; Helland et al., 2000) considered that the particles were distributed uniformly in the riser as an initial condition. This assumption is not realistic for predicting the cluster formation in CFB. In the particle-motion-resolved discrete model (Ouyang and Li, 1999), the interactions forces between particle and fluid, and vice versa, were considered separately which does not obey

Newton's third law. In the authors' opinion, this assumption is questionable since it is important to obey Newton's third law in the CFB system.

The purpose of this paper is to simulate a realistic process of cluster formation in CFB risers. In particular, we emphasis the influence of particle properties, porosity function and gas velocity on the global particle flow structure and the formation and development of local regions of higher particle concentration, i.e. "particle clusters".

In the model, the particle motion consists in collision steps and free flight steps. The particle interaction is described as instantaneous, binary and inelastic collision with friction, and not only by the fluid determines the flight step but also by its neighboring particles. The interaction forces between fluid and particle, and particle and fluid obey Newton's third law. The gas flow is calculated using Navier–Stokes' equations. Since collision between particles is the dominant interaction mechanism, we first describe the physics of collision. Then, fluid hydrodynamics and the computing method are presented. Finally, we comment our simulation results for CFB of particles in both homogeneous and heterogeneous (binary mixture) cases.

2. Particle dynamics

2.1. Treatment of collisions

The main assumptions of the collision model are:

- particles are spherical and quasi-rigid;
- collisions are binary and instantaneous with a contact point;
- interaction forces are impulsive and all other finite forces are negligible during collision;
- motion is two-dimensional with the particle mass centre moving in one plane;
- both the restitution and the friction coefficients are constant in a simulation.

The collision model used in this work follows mainly the methodology proposed by Wang and Mason (1992). Three parameters defining particle to particle and particle to wall interactions are introduced. First parameter is the coefficient of normal restitution, e ($0 \leqslant e \leqslant 1$), which characterizes the incomplete restitution of the normal component of the relative velocity at the contact point. Second parameter is the coefficient of dynamic friction ($\mu \geqslant 0$), which arises in collisions involving sliding. Finally, third parameter is the coefficient of tangential restitution, β_0 ($0 \leqslant \beta_0 \leqslant 1$), which arises in collisions, which return a fraction of the energy stored in the elastic deformation of both surfaces to the tangential component of the contact velocity.

The collision coordinate system used to describe the collision dynamics is defined in Fig. 1. The normal unit vector $\vec{n}$ at the contact point can now defined as

$$\vec{n} = \frac{\vec{r}_a - \vec{r}_b}{|\vec{r}_a - \vec{r}_b|} \tag{1}$$

where $\vec{r}_a$, $\vec{r}_b$ are the position vectors of particle a and b.

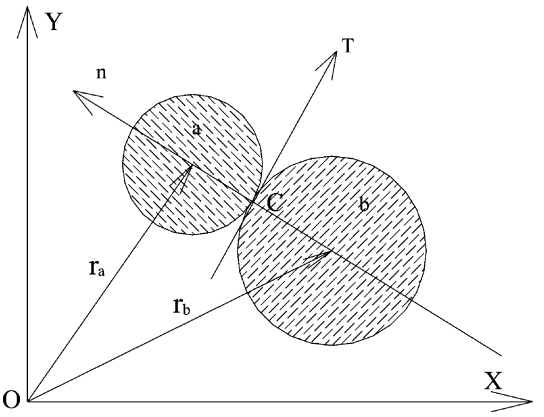

Fig. 1. Schematic illustration of the collision coordinate system.

For a binary collision of these spheres, applying Newton's second and third laws can derive the following equations:

$$m_a(\vec{v}_a - \vec{v}_{a,0}) = -m_b(\vec{v}_b - \vec{v}_{b,0}) = \vec{J} \tag{2}$$

$$\frac{I_a}{R_a}(\vec{\omega}_a - \vec{\omega}_{a,0}) = \frac{I_b}{R_b}(\vec{\omega}_b - \vec{\omega}_{b,0}) = -\vec{n} \times \vec{J} \tag{3}$$

where $I = (2/5)mR^2$ is the particle moment of inertia, $\vec{J} = \int_{t=0}^{t=t_c} \vec{F}_{ab}\,dt$, t_c is the contact time, R, m_p, v, ω are respectively the radius, mass, displacement velocity, rotational velocity of the particle, and F_{ab} is the impulsive force, $m_p = 4/3\,\pi R^3 \rho_p$, ρ_p is the particle density. Velocities prior to collision are indicated by the subscript 0.

The post-collision velocities of both particles can clearly be calculated when the impulse vector $\vec{J}$ is known. That-is-to say, if the force $\vec{F}_{ab}$ is known as a function of all involved parameters.

Firstly, the relative velocity at the contact point is defined as

$$\vec{v}_c = (\vec{v}_a - \vec{v}_b) - (R_a\vec{\omega}_a - R_b\vec{\omega}_b) \times \vec{n} \tag{4}$$

From the relative velocity, the tangential unit vector can be obtained:

$$\vec{\tau} = \frac{\vec{v}_{c,0} - \vec{n} \times (\vec{v}_{c,0} \cdot \vec{n})}{|\vec{v}_{c,0} - \vec{n} \times (\vec{v}_{c,0} \cdot \vec{n})|} \tag{5}$$

Eqs. (2) and (3) can be rearranged using the relation $(\vec{n} \times \vec{J}) \times \vec{n} = \vec{J} - \vec{n}(\vec{J} \cdot \vec{n})$, and Eq. (4) can now be expressed as follows:

$$\vec{v}_c - \vec{v}_{c,0} = B_1\vec{J} - (B_1 - B_2)\vec{n}(\vec{J} \cdot \vec{n}) \tag{6}$$

where

$$B_1 = \frac{7}{2}\left(\frac{1}{m_a} + \frac{1}{m_b}\right); \quad \text{and} \quad B_2 = \left(\frac{1}{m_a} + \frac{1}{m_b}\right)$$

At this point, the following constitutive relations are used to close the above equations:

(1) Coefficient of (normal) restitution: $\vec{v}_c \cdot \vec{n} = -e(\vec{v}_{c,0} \cdot \vec{n})$.
(2) Coefficient of dynamic friction: $|\vec{n} \times \vec{J}| = -\mu(\vec{n} \cdot \vec{J})$.
(3) Coefficient of (tangential) restitution: $\vec{n} \times \vec{v}_c = -\beta_0(\vec{n} \times \vec{v}_{c,0})$.

Notice that the third relation does not affect the components parallel to $\vec{n}$ and that the components orthogonal to $\vec{n}$ are related by a factor β_0. Combining Eqs. (4) and (5) yields to the following expression for the normal component of the impulse vector:

$$\vec{J}_n = -(1+e)\frac{\vec{v}_{c,0} \cdot \vec{n}}{B_2} \tag{7}$$

For the tangential component, two types of collisions can be distinguished that are called sticking and sliding, whether the initial slip between the particle surfaces ceases or not. As shown by Wang and Mason (1992), the criterion to determine the type of collision is as follows:

$$\begin{aligned} \mu &< \frac{(1+\beta_0)\vec{v}_{c,0} \cdot \vec{\tau}}{\vec{J}_n B_1} \quad \text{sliding} \\ \mu &\geqslant \frac{(1+\beta_0)\vec{v}_{c,0} \cdot \vec{\tau}}{\vec{J}_n B_1} \quad \text{sticking} \end{aligned} \tag{8}$$

For collisions of sticking type, the tangential impulse is given by

$$\vec{J}_\tau = -(1+\beta_0)\frac{|\vec{n} \times \vec{v}_{c,0}|}{B_1} = -(1+\beta_0)\frac{\vec{v}_{c,0} \cdot \vec{\tau}}{B_1} \tag{9}$$

For collisions of sliding type, the tangential impulse is given by

$$\vec{J}_\tau = -\mu\vec{J}_n \tag{10}$$

The post-collision velocities can be calculated from Eqs. (2) and (3).

In particle to wall collisions, the mass of particle a or b is infinitely large and the velocity vectors are all set equal to zero.

2.2. Sequence of collisions

Two main ways were proposed to account for inter-particle collisions; they are stochastic and deterministic approaches. The stochastic procedure is based on selecting randomly a pair of particles which are located in the same cell, and then computing a collision probability for this selected pair and carrying out the collision according to the acceptance–rejection method (Bird, 1989; Illner and Neunzert, 1987). Few researchers used this approach to investigate the hydrodynamics in vertical or horizontal pipes (Tanaka and Tsuji, 1991; Wassen and Frank, 2001). With the rapid increase of computer power, the deterministic approach was used widely in the last few years (Hoomans et al., 1996; Helland et al., 2000). In the deterministic process, the position and velocity of each pair of particles in the flow field must be checked in order to define the minimum

collision time. The most interesting feature of the approach is that it is very convenient to determine the collision time of a pair of different particles. Obviously, this way of treating collisions consumes computer time because the collision time is proportional to the square of the total number of particles.

The collision time of a particles pair is defined as the time interval until collision. It can be calculated from the initial position and velocity vectors of both particles (Allen and Tildesly, 1980):

$$t_{ab} = \frac{-\vec{r}_{ab} \cdot \vec{v}_{ab} - \sqrt{(\vec{r}_{ab} \cdot \vec{v}_{ab})^2 - \vec{v}_{ab}^2(\vec{r}_{ab}^2 - (R_a + R_b)^2)}}{\vec{v}_{ab}^2} \tag{11}$$

where t_{ab} is the collision time, $\vec{v}_{ab} = \vec{v}_a - \vec{v}_b$ and $\vec{r}_{ab} = \vec{r}_a - \vec{r}_b$ are the relative velocity and position of particles.

If $\vec{r}_{ab} \cdot \vec{v}_{ab>0}$, the particle are moving away from each other and they will not collide. In the case of a collision with a wall, the collision time depends simply on the distance to the wall and on the normal velocity component toward this wall.

2.3. Forces acting on a particle

The motion of every single particle in the flow between two collisions is subject to Newton's equation of motion. Magnus force, Saffman force, Basset, and the unsteady force are neglected due to the high ratio of particle density to gas density. Consequently, the particle motion in suspension is governed by gravity and drag force:

$$\frac{\mathrm{d}\vec{v}_p}{\mathrm{d}t} = \vec{g} + \frac{\vec{F}_d}{m_p} - \frac{V_p}{m_p}\nabla p \tag{12}$$

where g is gravitational acceleration, $\vec{F}_d$ is drag force, $V_p = 1/6\,\pi d_p^3$ is the volume of a particle, d_p is the particle diameter, p is the fluid pressure. The third term at the right represents the pressure gradient force, which can be neglected with respect to the drag force in CFB (Ouyang and Li, 1999; Helland et al., 2000).

The drag force on a suspended particle is given by

$$\vec{F}_d = \frac{1}{8}\pi d_p^2 C_d' \rho_g \varepsilon^2 |\vec{u} - \vec{v}_p|(\vec{u} - \vec{v}_p) \tag{13}$$

where ε is the porosity, C_d' is the effective drag coefficient, $\vec{u}$ is the gas velocity, $\vec{v}_p$ is the particle velocity, and ρ_g is the gas density.

The effective drag coefficient C_d' depends strongly on the local void fraction in the vicinity of the considered particle. According to Wen and Yu (1966), it can be written as

$$C_d' = C_d \varepsilon^{-n} \tag{14}$$

where n is the porosity factor.

The drag coefficient C_d for an isolated particle depends on the particle Reynolds number as given by Rowe and Henwood (1961):

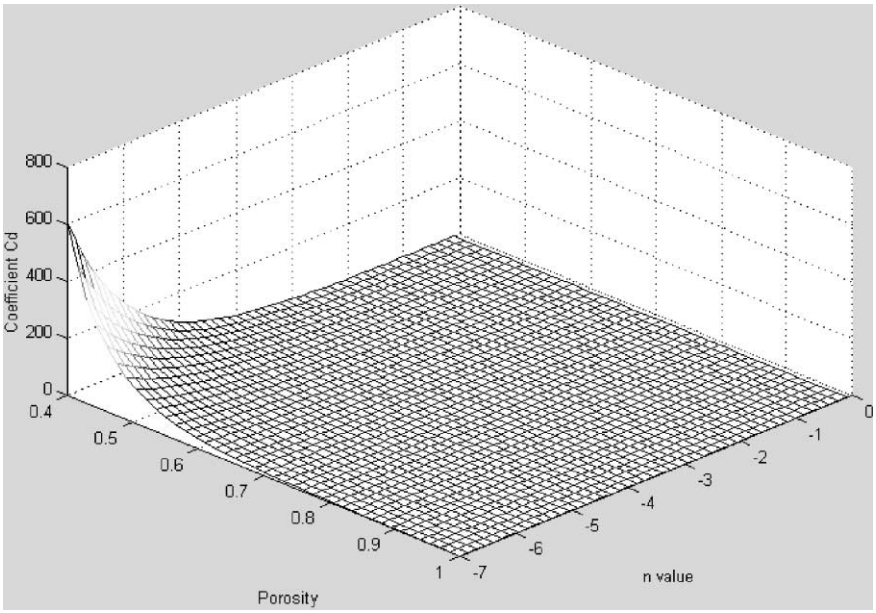

Fig. 2. Relation between n and C'_{d}.

$$C_{\mathrm{d}} = \begin{cases} \frac{24}{Re_{\mathrm{p}}}(1 + 0.15Re_{\mathrm{p}}^{0.687}) & Re_{\mathrm{p}} < 1000 \\ 0.44 & Re_{\mathrm{p}} \geqslant 1000 \end{cases} \tag{15}$$

where the particle Reynolds number Re_{p} is defined as

$$Re_{\mathrm{p}} = \frac{\varepsilon\rho_{\mathrm{g}}|\vec{u} - \vec{v}_{\mathrm{p}}|\,\mathrm{d}_{\mathrm{p}}}{\mu_{\mathrm{g}}} \tag{16}$$

where μ_{g} is the gas shear viscosity.

Eq. (14) shows that the drag force on a suspended particle depends on the porosity and on n value. Many discussions on n value can be found in literature (Richardson, 1971; Gibilaro et al., 1987; Haider and Levenspiel, 1989). In a gas–solid system, it has been found that n may reach 9, depending on the sphericity and the physical properties of the particle. Experimental results proposed higher n values for non-spherical and for size-distributed particles. The relationship between $C'_{\mathrm{d}} \propto \varepsilon^{-n}$ is shown in Fig. 2, the strong non-linearity of the drag force with porosity is the most important trend.

3. Gas-phase hydrodynamics

3.1. Governing equations

The gas motion follows a generalization of Navier–Stokers' equations for gas interacting with solids, leading to the following equations for mass and momentum conservation in vector form:

Continuity equation:

$$\frac{\partial(\varepsilon\rho_g)}{\partial t} + (\nabla \cdot \varepsilon\rho_g \vec{u}) = 0 \tag{17}$$

Momentum equation:

$$\frac{\partial(\varepsilon\rho_g \vec{u})}{\partial t} + (\nabla \cdot \varepsilon\rho_g \vec{u}\vec{u}) = -\varepsilon\nabla p + \vec{F}_{p-g} - (\nabla \cdot \varepsilon\bar{\bar{\tau}}_g) + \varepsilon\rho_g \vec{g} \tag{18}$$

where $\vec{F}_{p-g}$ and $\bar{\bar{\tau}}$ are respectively volumetric particle–fluid interaction force and viscous stress tensor. The fluid viscous stress tensor is given by an expression analogous to that for a Newtonian fluid (Anderson and Jackson, 1967), that is

$$\bar{\bar{\tau}} = \left[\left(\mu'_f - \frac{2}{3}\mu_f\right)\nabla \cdot u\right]\delta_{kk} + \mu_f[(\nabla u) + (\nabla u)^{-1}] \tag{19}$$

where δ_{kk} is the Kronecker delta, and μ'_f is the fluid bulk viscosity. Under the present simulation conditions, μ'_f can be neglected (Bird et al., 1960).

3.2. Interaction force

As the fluid drag force acting on each particle is known, according to Newton's third law of motion, the volumetric fluid–particle interaction force can be determined by

$$\vec{F}_{p-g} = -\frac{\sum_{i=1}^{k_c} \vec{F}_d}{\Delta V} \tag{20}$$

where ΔV is the volume of a computational cell, and k_c is the number of particles in the cell. The volume is taken to be equal to $DX \cdot DY \cdot \bar{d}_p$ (where DX and DY are the X and Y dimensions of a computational cell), $\bar{d}_p$ is the simple mean value of the particle diameter in the considered computational cell of the discrete particle model:

$$\bar{d}_p = \frac{\sum_{i=1}^{k''} d_p}{k''} \tag{21}$$

where k'' is particle number in a computational cell.

3.3. Calculation of porosity

For each cell of the computational domain, porosity can be calculated on the basis of the area occupied by the particles in the cell. Eq. (14) shows that porosity is a very important parameter which influences strongly both the gas-phase and the solid phase motions. The voidage is obtained by subtracting the sum of the particle volumes from the volume of a fluid cell. When a particle overlaps one neighboring cell or more, the volume fraction included in a particular fluid cell is taken into account to calculate the voidage of the cell. The porosity in the cell is

$$\varepsilon_{2D} = 1 - \frac{\sum_i^{k_c} S_i}{\Delta S} \tag{22}$$

The porosity calculated by Eq. (22) is based on a 2D analysis. Therefore, it is inconsistent with the applied empiricism in the calculation of the drag force exerted on a particle and of the interfacial friction, since actually the relevant correlations are based on 3D systems. In order to be more consistent, we used a 3D porosity (ε_{3D}) deduced from that calculated on area basis (ε_{2D}) by (Ouyang and Li, 1999):

$$\varepsilon_{3D} = 1 - \frac{\sqrt{2}}{\sqrt{\pi\sqrt{3}}}(1 - \varepsilon_{2D})^{3/2} \tag{23}$$

4. Computational method

- The particle motion was divided in two steps: collision step and free flight step. The former is controlled by the dynamics of collision as described in Section 2.1, the latter is controlled by Eq. (12).
- Start: setting randomly some particles at the bottom of the riser, and causing a small disturbance obtained as initial conditions. Then, the particles began to move because of the gas flow, which was injected into the riser uniformly from the bottom.
- There was no obstacle at the exit, and consequently the particles were free to leave with gas flow. The inlet solid flux was set constant. Therefore, the simulated process is similar to a practical CFB riser, in which the particle number varies with time.

Table 1
Physical and numerical simulation parameters

Properties	Value
Bed height, H	37.8 cm
Bed width, W	7.0 cm
Temperature in the riser, T	1123 K
Gas density, ρ_g	0.32 kg/m^3
Kinetic viscosity of gas, μ_g	4.552×10^{-5} kg/(m s)
Gas bulk velocity, u	6.5 and 7.2 m/s
Particle diameter, d_p	
Sand, d_s	0.7 mm
Alumina, d_a	1.2 mm
Particle apparent density, ρ_p	
Sand, ρ_s	2650.0 kg/m^3
Alumina, ρ_a	1350.0 kg/m^3
Coefficient of restitution for particle–particle/wall collision, e	0.9 and 1.0
Coefficient of friction for particle–particle/wall collision, μ	0.3 and 0.0
n value	4.7 and 2.3
Number of grid cells, $I \times J$	22×44
Initial particle number in the riser	748
Mass loading ratio at the inlet cell	0.1 kg(particle)/kg(gas)
Total number of simulated particles in the riser	>7000
Time step of gas, t	5.0×10^{-5} s

- Using a "nearest neighbor list" saved substantial CPU time. When looking for a collision partner for a particle, only the particles in the neighbor list must be scanned. We chose the diameter of the neighbor list to be five times that of the particle.
- The conventional SIMPLE (semi-implicit method for pressure-linked equations) method (Patankar, 1980) was used to solve the equations for the fluid phase. The governing equations were discretized in finite volume form on a uniform, staggered grid. The second-order central difference scheme was used for the pressure gradient and divergence terms. The first-order up-wind scheme for the convection term and a second-order Crank–Nicholson scheme for the time derivative were used, respectively.
- Boundary conditions: For the fluid velocity, the no-slip boundary condition was applied to left and right walls, and zero normal gradient condition was set to the top exit. At the inlet cell, fluid velocity was imposed. For the porosity and pressure correction, the zero normal gradient condition was used along the boundaries. The pressure, which was obtained from the pressure correction at all inner points, was calculated on the boundaries by using a second-order extrapolation from the inner points.
- Computation procedure: After the main loop initialisation, the calculation continued until the time exceeds the specified end time. Within the loop, the forces acting on a particle were calculated first. Knowing the particle velocities and positions, a sequence of collisions was processed, where the dynamics of a single collision was calculated using the collision model. At the end of

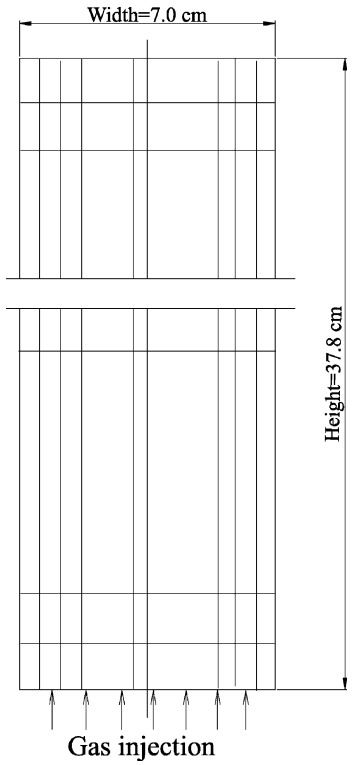

Fig. 3. Calculation domain and grid arrangement of the simulation.

this step, the particle position and velocity were known. After calculating the cell porosity and the force acting on the gas, the gas flow field was obtained by solving Navier–Stokes' equations. Finally, the user specified data were saved in the output.

- Computation conditions: Both computation conditions and physical and additional parameters used are displayed in Table 1. The simulated CFB consists in a rectangular container of 7.0 cm width and 37.8 cm height. The calculation domain and the grid arrangement are shown in Fig. 3.

5. Results and discussion

5.1. Sensitivity to model parameters

A sensitivity analysis was performed to investigate the influence of the three key parameters: the restitution coefficient, e, the friction coefficient, μ, and the porosity factor n. In all these simulations, other conditions were identical (Table 1).

Figs. 4–6 show time series of particle structures and the velocity distribution of the gas phase in the riser for different parameters values. They clearly demonstrate that the results are highly sensitive to the restitution and friction coefficients to the porosity factor. In the case of ideal particles ($e = 1.0$, $\mu = 0.0$), a rather homogeneous dispersion of particles and almost no cluster formation in the riser can be observed. In the case of more realistic interactions between particles

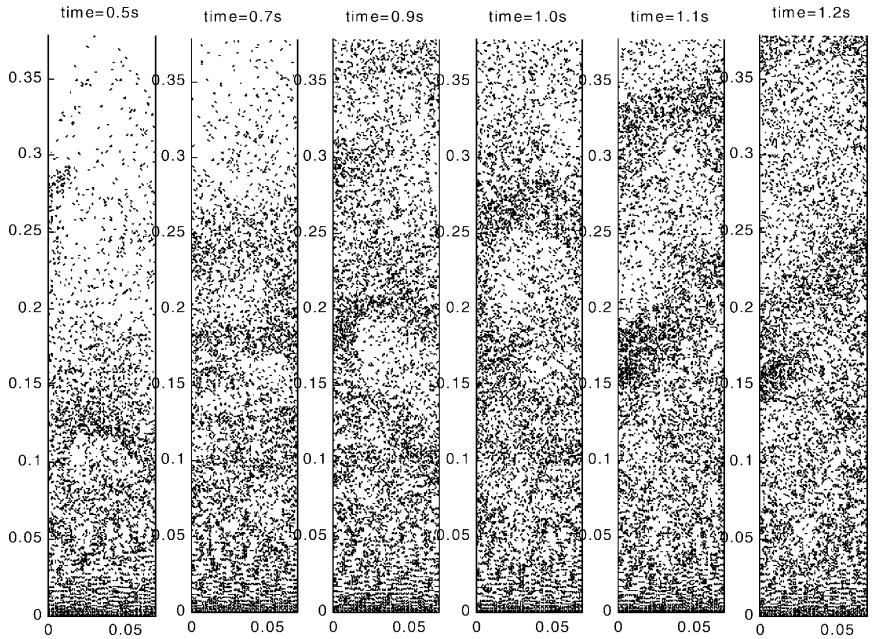

Fig. 4. Time series of particle structure in the riser ($\mu = 0.0$, $e = 1.0$, $n = 4.7$, $\rho_p = 2650$ kg/m^3, $d_p = 0.7$ mm, $u_g = 6.5$ m/s).

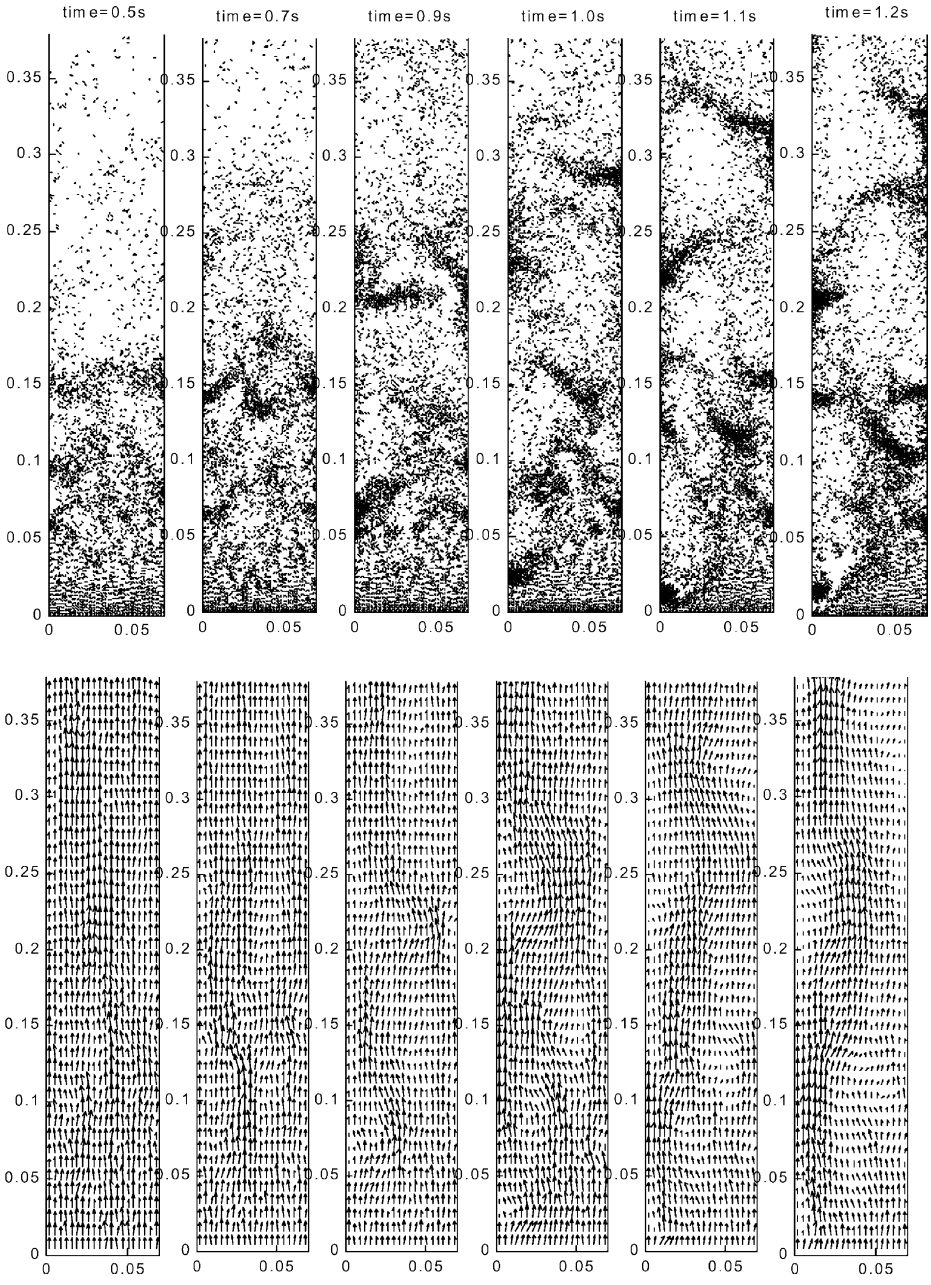

Fig. 5. Time series of particle structure and velocity distribution of the gas phase in the riser ($\mu = 0.3$, $e = 0.9$, $n = 4.7$, $\rho_p = 2650$ kg/m^3, $d_p = 0.7$ mm, $u_g = 6.5$ m/s).

($e = 0.9$, $\mu = 0.3$), a heterogeneous distributions of particles with formation of clusters at various levels in the riser. When $n = 2.3$, the clusters are also formed but their formation and disap-

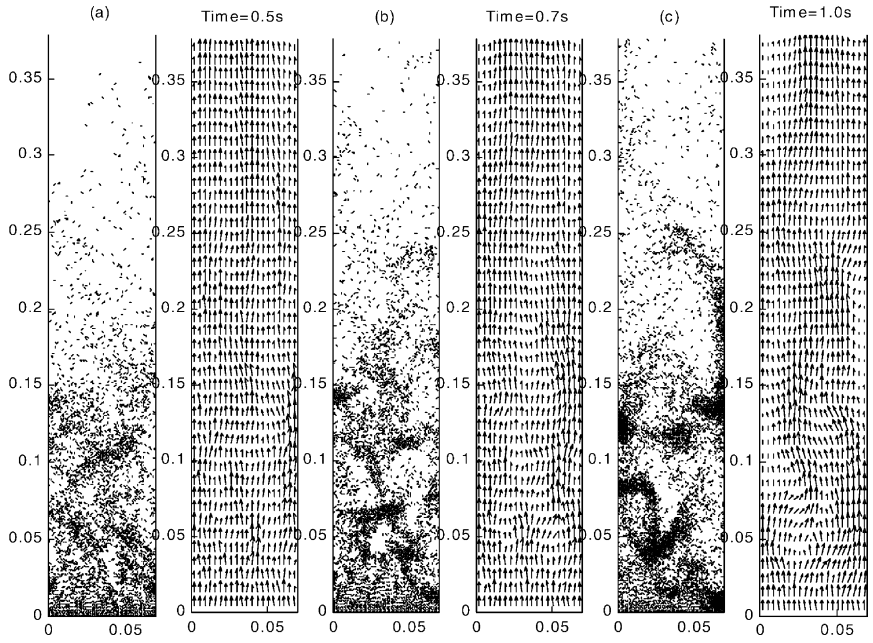

Fig. 6. Time series of particle structure and velocity distribution of the gas phase in the risers ($\mu = 0.3$, $e = 0.9$, $n = 2.3$, $\rho_p = 2650$ kg/m^3, $d_p = 0.7$ mm, $u_g = 6.5$ m/s).

pearance are much slower than for $n = 4.7$, because the forces acting on the particles decrease (see in Fig. 2). It can also be seen on the figures that the gas flows towards the regions of high porosity. Highly preferential flow leads to a very strong non-uniform fluid drag force in the riser, which in turn affects greatly the particle structures. Fig. 7 shows the distributions of the particle kinetic energy and velocity for elastic (Fig. 7a–c) and non-ideal particles (Fig. 7d–f). Most particles move upward for elastic collisions, whereas a lot of them move downward for non-ideal collisions. The kinetic energy distribution of elastic particles is more uniform than that of non-ideal particles. Kinetic and rotational energy of the particles is partially dissipated during collisions of non-ideal particles. This means that their velocity after impact is smaller than in the ideal case, thus leading to configuration where particles are less spaced, resulting in a lower porosity value. Eqs. (13) and (14) show that the lower the porosity the higher the drag force, which results in the particles movement upward. However, as shown in Figs. 4–6, a lower porosity also results in gas phase movement around the cluster, thus reducing the drag force on the particle because of the decrease of relative velocity between gas and particle (see Eq. (13)). The force increase due to the porosity decrease is lower than the force decrease due to the reduction of the relative velocity. Consequently, the particle vertical velocity decreases.

Fig. 8 shows the variation of particle number with time in both ideal and non-ideal cases. The final particles number injected into the bed is more than 7000. First, there is no difference between ideal and non-ideal cases. Then when time increases, elastic particles are flowed out of the riser more than non-ideal particles. Clearly, the circulating rate in CFB depends on the particle properties.

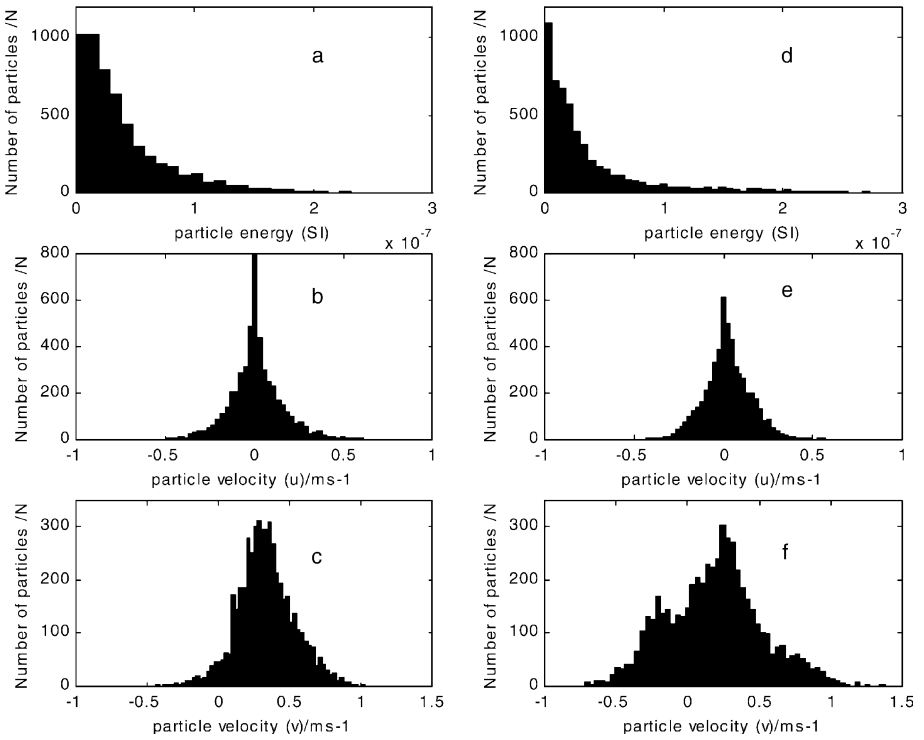

Fig. 7. Comparisons of the distribution of the particles kinetic energy and velocity for elastic (a,b,c) and inelastic particle (d,e,f).

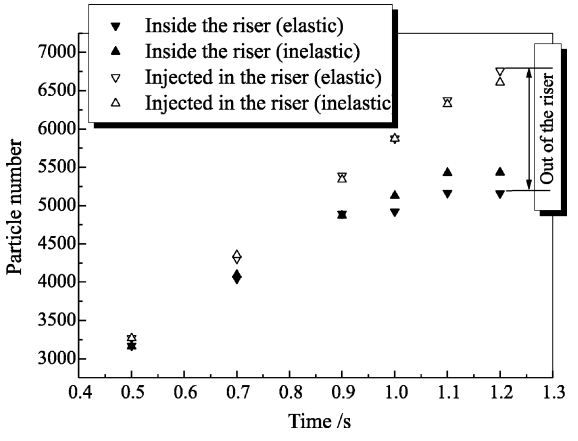

Fig. 8. Variation of particle number injected in and staying inside the riser with time.

Fig. 9 illustrates the source terms in the momentum equation for u and v directions. Both of them are large and unevenly distributed. As argued above, the algorithm is able to converge,

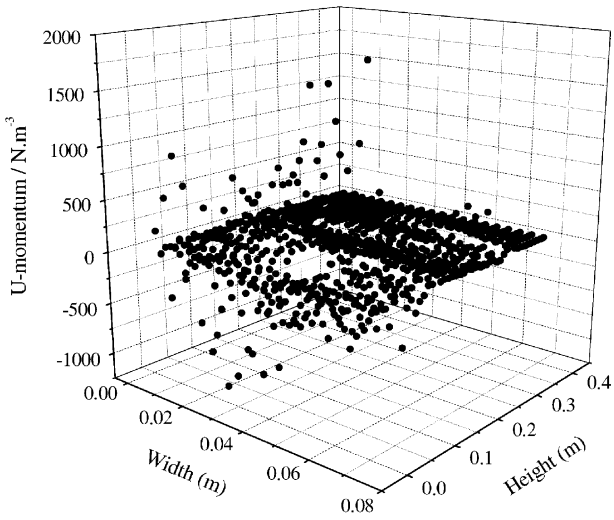

(a)

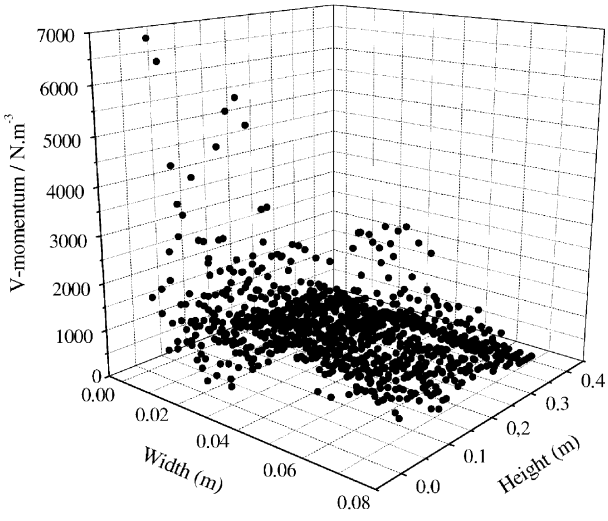

(b)

Fig. 9. u and v source terms (a) u direction, (b) v direction.

whereas, in order to improve the convergence, previous researchers used special calculation algorithms taking into account the unevenly distributed source terms (Paulsen and Holst, 1995).

5.2. Binary mixtures

First, we studied two types of binary mixture of particles: same density and different size, and same size and different density (with $d_1/d_2 = \rho_1/\rho_2$). Fig. 10, plotting the ratio of the particle

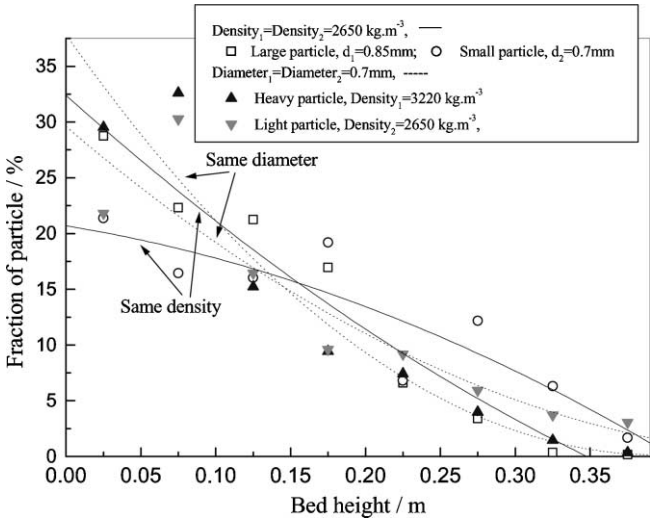

Fig. 10. Particle distribution along the riser ($t = 1$ s). Case: same density different diameter and same diameter different density.

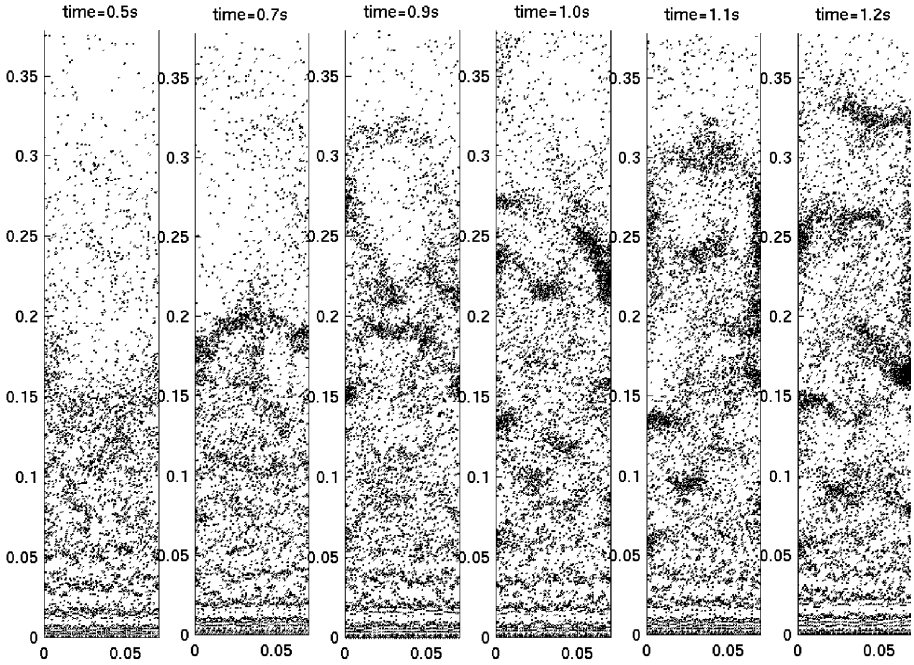

Fig. 11. Time series of particle structure in the riser ($\mu = 0.3$, $e = 0.9$, $n = 4.7$, $\rho_p = 2650$ kg/m^3, $d_p = 0.7$ mm, and $\rho_p = 1350$ kg/m^3, $d_p = 1.2$ mm, $u_g = 6.5$ m/s).

number of one class at a given height to the total particle number of this class versus the bed height, shows that all the large/heavy particles remain in the riser, whereas 15–16% of the small/

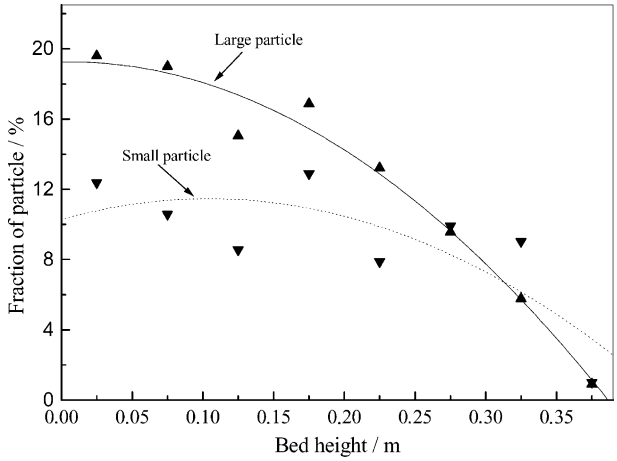

Fig. 12. Particle distribution along the riser ($t = 1.2$ s). Case: different density and diameter.

light particles flow out. A tendency to segregate seems to appear with the mixture of two-diameter particles.

The second case considered a binary mixture of particles different in both size and density, the diameters and density being correlated by $\rho_s d_s = 1.15\rho_b d_b$. Fig. 11 illustrates time series of flow structure for the system with gas velocity $u_g = 6.5$ m/s. It shows a heterogeneous distribution of particles with clusters displacement at various levels in the riser. All the injected large particles remain in the riser, whereas 16.1% of small particles flow out. Fig. 12 shows the particle distribution in the riser. The particles behave differently in the system: small particles are rather evenly distributed in the bed, whereas the big ones tend to accumulate in the lower part of the bed. This could be the first step towards segregation, which actually requires much longer time to occur. For gas velocity slightly higher ($u = 7.2$ m/s), most particles are still distributed heterogeneously, but the distribution is more uniform. The higher velocity results in higher drag force on the particles, thus particles moving faster and then higher kinetic energy, which easily destruct the "initial cluster" (small cluster with several particles), and therefore the probability of cluster formation decreases. The flow structures agree with those observed by Tanaka and Tsuji (1991) and Yonemura et al. (1993).

5.3. Cluster formation and disappearance

Fig. 13 is a snapshot of the local gas velocity, and particle structure (a) and particle velocity (b) in the lower part of the riser. The structure changes rapidly with time. The particle velocity is much smaller in the cluster than in the region of higher porosity due to the non-uniform distribution of gas velocity caused by the particle flow pattern. A few particles move around the clusters with high velocity and others collide with the cluster. Therefore, the cluster either captures them or they destruct it. Some particles move apart from the wake of the cluster, which causes its disappearance.

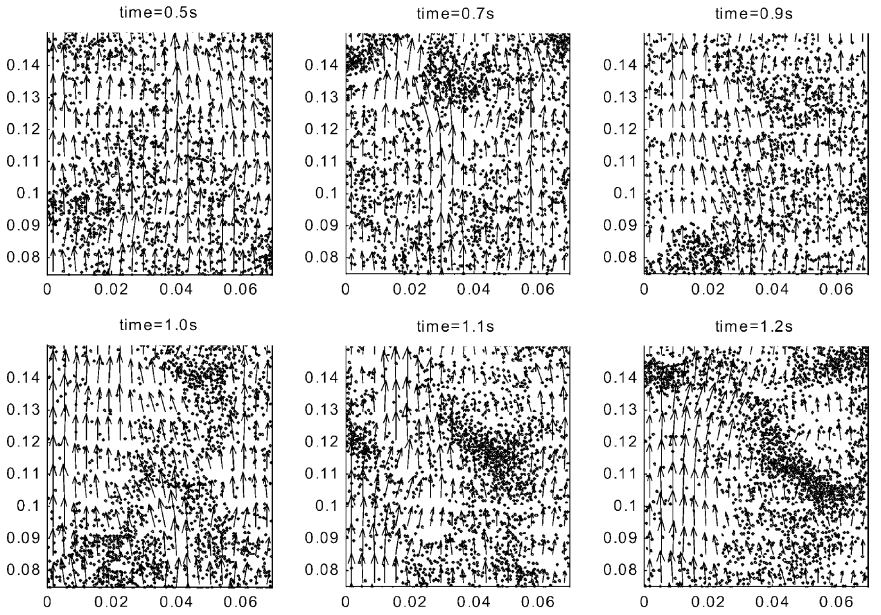

(a)

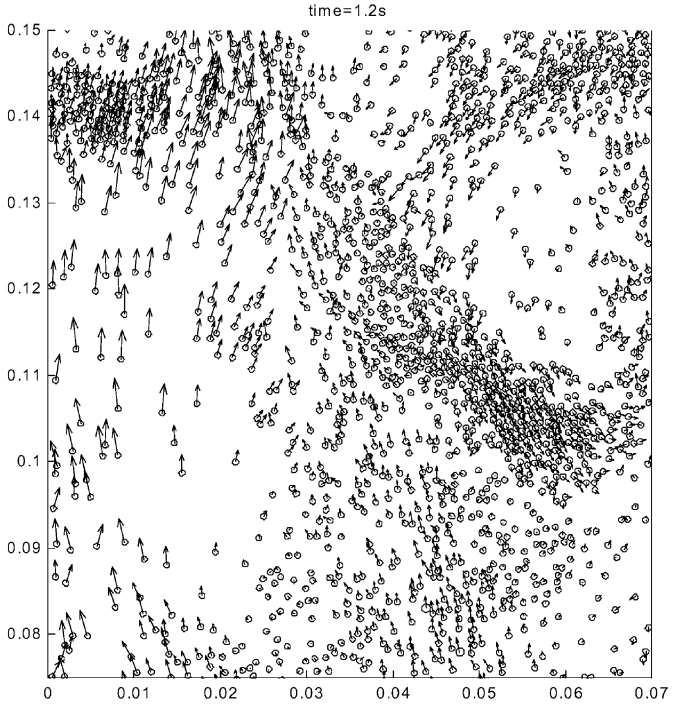

(b)

Fig. 13. Snapshot of the gas velocity, particle structure (a), and particle velocity ($t = 1.2$ s) in the riser between 0.075 and 0.15 cm (corresponding to Fig. 5).

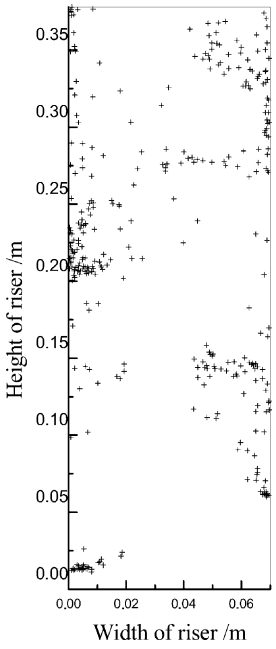

Fig. 14. Final positions of initial particles after 1.2 s.

Fig. 14 shows the final ($t = 1.2$ s) position of the particles set initially inside the riser (corresponding to Fig. 5). After 1.2 s, half the particles have been flowed out of the riser (55.7%). It is interesting to notice that some particles are still remaining at the bottom of the riser although they were set in the riser at initial time. The particles move irregularly, which is favorable to particles mixing in the riser, and they tend to move toward the wall.

6. Conclusions and future work

We have investigated the influence of the collision parameters (from ideal to realistic particles), of the porosity factor, and of the particle density on the global and local flow structures in a 2D CFB riser. We found that the particle–particle and particle–wall collisions together with the gas particle interaction dominate the formation of heterogeneous particle flow structures, especially the formation of clusters. In terms of kinetic energy and velocity distribution, the difference between ideal and non-ideal particles results in relatively homogeneous and heterogeneous particle flow structures, and the porosity function has significant effect on the structures. The gas flows preferentially in the region of high porosity, which leads to non-uniform drag force on the particles and affects strongly the particle flow structures. When fluidizing a binary mixture, segregation is predicted. The examination of the cluster microstructure shows that the particle velocity inside the cluster is smaller than around it.

In fact, both theoretical analysis and experimental results (Zelenko et al., 1996; Zhou et al., 2000) showed that turbulence is another main reason, which dominates the particle flow structure

in the CFB riser. Consequently, further analytical and numerical works are currently developed to achieve more realistic simulations of turbulent flow.

Acknowledgements

We are grateful to AFCRST (Association Franco-Chinoise pour la Recherche Scientifique et Technique) and ADEME (Agence de l'Environment et de la Maîtrise de l'Energie) for financial assistance.

References

Allen, M.P., Tildesly, D.J., 1980. Computer simulation of liquids. Oxford University Press, Oxford.

Anderson, T.B., Jackson, R., 1967. A fluid mechanical description of fluidized beds. I & EC Fundam. 6, 527–539.

Bader, R., Findlay, J., Knowlton, T.M., 1988. Gas/solid flow patterns in a 30.5 cm diameter circulating fluidized bed. In: Basu, P., Large, J.F. (Eds.), Circulating Fluidized Bed II. Pergamon, New York, pp. 123–137.

Bird, G.A., 1989. Perception of numerical methods in rarefield gas dynamics. Progr. Astro. Aero. 118, 211–226.

Bird, R.B., Stewart, W.E., Lightfood, E.N., 1960. Transport Phenomena. Wiley, New York.

Bolio, E.J., Yasuna, J.A., Sinclair, J.L., 1995. Dilute turbulent gas–solid flow in risers with particle–particle interactions. AIChE J. 41, 1375–1386.

Cao, J., Ahmadi, G., 1995. Gas-particle two-phase turbulent flow in a vertical duct. Int. J. Multiphase Flow 21, 1203–1228.

Gauthier, D., Zerguerras, S., Flamant, G., 1999. Influence of the particle size distribution of powders on the velocities of minimum and complete fluidization. Chem. Eng. J. 74, 181–196.

Gibilaro, L.G., Foscolo, P.U., Waldram, S.P., Felice, R.D., Hossain, I., 1987. A review of applications of a fluid–particle interaction model to predictions of fluidized bed behavior. Chem. Eng. Commun. 62, 17–29.

Gidaspow, D., Tsuo, Y.P., Luo, K.M., 1989. Computed and experimental cluster formation in velocity profiles in circulating fluidized beds. In: Grace, J.R., Shemilt, L.W., Bergougnou, M.A. (Eds.), Fluidization VI. Engineering Foundation, New York, pp. 81–88.

Haider, A., Levenspiel, O., 1989. Drag coefficient and terminal velocity of spherical and nonsphericial particles. Powder Technol. 58, 63–70.

Helland, E., Occelli, R., Tadrist, L., 2000. Numerical study of cluster formation in a gas-particle circulating fluidized bed. Powder Technol. 110, 210–221.

Hoomans, B.P.B., Kuipers, J.A.M., Briels, W.J.W., Van Swaaij, P.M., 1996. Discrete particle simulation of bubble and slug formation in a two-dimensional gas-fluidized bed: a hard-sphere approach. Chem. Eng. Sci. 51, 99–118.

Hoomans, B.P.B., Kuipers, J.A.M., Mohd Salleh, M.A., Stein, M., Seville, J.P.K., 2001. Experimental validation of granular dynamics simulations of gas-fluidised beds with homogeneous in-flow conditions using positron emission particle tracking. Powder Technol. 116, 166–177.

Horio, M., Kuroki, H., 1994. Three dimensional flow visualization of dilutely dispersed solids in bubbling and circulating fluidized beds. Chem. Eng. Sci. 49, 2413–2428.

Illner, R., Neunzert, H., 1987. On simulation methods for the Boltzmann equation. Transport Theory Stat. Phys. 16, 141–154.

Ito, M., Tsukada, M., Shimamura, J., Horio, M., 1998. Prediction of cluster size and slip velocity in circulating fluidized beds by a DSMC model. In: Fan, L.-S., Knowlton, T.M. (Eds.), Fluidization IX. Engineering Foundation Inc., New York, pp. 525–532.

Kuipers, J.A.M., Van Duin, K.J., Van beckum, F.P.H., Van Swaaij, W.P.M., 1992. A numerical model of gas-fluidized beds. Chem. Eng. Sci. 51, 4087–4102.

Kumaran, V., Koch, D.L., 1993. Properties of a bidisperse particle–gas suspension Part 1. Collision time small compared with viscous relation time. J. Fluid Mech. 247, 623–645.

Mathiesen, V., Solberg, T., Hjertager, B.H., 2000. Predications of gas/particle flow with an Eulerian model including a realistic particle size distribution. Powder Technol. 112, 34–45.

Ouyang, J., Li, J., 1999. Discrete simulations of heterogeneous structure and dynamic behavior in gas–solid fluidization. Chem. Eng. Sci., 5427–5440.

Patankar, S.V., 1980. Numerical heat transfer and fluid flow. Hemisphere, New York, USA.

Paulsen, B.B., Holst, M.D., 1995. Lagrangian predication of particulate two-phase flows at high particle loadings. Available from <http://www.iet.auc.dk/afd2/online.pub/article.2>.

Richardson, J.F., 1971. In: Davidson, J.F., Harrison, D. (Eds.), Fluidization. Academic Press, London (Chapter 2).

Rowe, P.N., Henwood, G.A., 1961. Drag force in a hydraulic model of a fluidized bed-part 1. Trans. Instn. Chem. Eng., 39–43.

Tanaka, T., Tsuji, Y., 1991. Numerical simulation of gas–solid two-phase flow in a vertical pipe: on the effect of inter-particle collision. In: Gas–Solid Flows, vol. 121. ASME FED, pp. 123–128.

Tanaka, T., Yonemura, S., Tsuji, Y., 1995. Effects of particle properties on the structure of cluster. In: Gas-Particle Flows, vol. 228. ASME (FED), pp. 297–302.

Tsuji, Y., Kawaguchi, T., Tanaka, T., 1993. Discrete particle simulation of two-dimensional fluidized bed. Powder Technol. 77, 79–87.

Van Wachem, B.G.M., Schouten, J.C., Van den Bleek, C.M., Krishna, R., Sinclair, J.L., 2001a. CFD modelling of gas-fluidized beds with a bimodal particle mixture. AIChE J., 1292–1301.

Van Wachem, B.G.M., Van der Schaff, J., Schouten, J.C., Krishna, R., Van den Bleek, C.M., 2001b. Experimental validation of Lagrangian–Eulerian simulations of fluidized beds. Powder Technol. 116, 155–165.

Wang, Y., Mason, M.T., 1992. Two-dimensional rigid-body collisions with friction. J. Appl. Mech. 59, 635–642.

Wassen, E., Frank, Th., 2001. Simulation of cluster formation in gas–solid flow induced by particle–particle collisions. Int. J. Multiphase Flow 27, 437–458.

Wen, C.Y., Yu, Y.H., 1966. Mechanics of fluidization. Chem. Eng. Prog. Symp. Ser. 62, 100–108.

Xu, B.H., Xu, A.B., 1997. Numerical simulation of the gas–solid flow in a fluidized bed by combining discrete particle method with computational fluid dynamics. Chem. Eng. Sci. 52, 2785–2809.

Yerushalmi, J., Cankurt, M., Geldart, D., Liss, B., 1978. Flow regimes in vertical gas–solid contact systems. AIChE Symp. Ser. 74, 1–12.

Yonemura, S., Tanaka, T., Tsuji, Y., 1993. Cluster formation in gas–solid flow predicated by the DSMC method. In: Gas Solid Flows, 166. ASME FED, pp. 303–309., Book No. H008062.

Zelenko, V.L., Sergeev, Y.A., Tjin, T., Iske, P.L., 1996. Clusters and particle segregation in gas–solid flow through a vertical tube. Physica A 226, 274–294.

Zhou, H.S., Lu, J.D., Lin, L., 2000. Turbulence structure of the solid phase in transition region of a circulating fluidized bed. Chem. Eng. Sci. 55, 839–847.